CELLULAR NEUROSCIENCE

Network-driven intracellular cAMP coordinates circadian rhythm in the suprachiasmatic nucleus

Daisuke Ono[1,2]*, Huan Wang[3], Chi Jung Hung[1,2], Hsin-tzu Wang[4,5,6], Naohiro Kon[4,5], Akihiro Yamanaka[7], Yulong Li[3], Takashi Sugiyama[8]

The mammalian central circadian clock, located in the suprachiasmatic nucleus (SCN), coordinates the timing of physiology and behavior to local time cues. In the SCN, second messengers, such as cAMP and Ca^{2+}, are suggested to be involved in the input and/or output of the molecular circadian clock. However, the functional roles of second messengers and their dynamics in the SCN remain largely unclear. In the present study, we visualized the spatiotemporal patterns of circadian rhythms of second messengers and neurotransmitter release in the SCN. Here, we show that neuronal activity regulates the rhythmic release of vasoactive intestinal peptides from the SCN, which drives the circadian rhythms of intracellular cAMP in the SCN. Furthermore, optical manipulation of intracellular cAMP levels in the SCN shifts molecular and behavioral circadian rhythms. Together, our study demonstrates that intracellular cAMP is a key molecule in the organization of the SCN circadian neuronal network.

INTRODUCTION

The circadian clock coordinates the timing of physiology and behavior. In mammals, the suprachiasmatic nucleus (SCN) of the hypothalamus plays a crucial role in the regulation of rhythmic physiological functions such as sleep and wakefulness. Individual SCN neurons show intrinsic circadian rhythms that are considered to be regulated by transcription-translation negative feedback loops (TTFLs) involving clock genes, whereby protein products from *Period* (*Per*) and *Cryptochrome* (*Cry*) genes periodically suppress their own gene expression (*1*). A variety of real-time recording methods have revealed the existence of cellular circadian rhythms in spontaneous firing, gene expression, and protein levels in the SCN (*2*–*4*). Circadian rhythms of individual cells within the SCN network synchronize with one another via neuronal and humoral factors to increase the robustness and stability of the ensemble output (*5*, *6*). Thus, the SCN neuronal network plays a critical role in integrating and transducing rhythms of individual oscillators to overt and stable outputs that time physiology and behavior.

Second messengers such as cyclic adenosine monophosphate (cAMP) and Ca^{2+} play a variety of roles in biological functions by transmitting and amplifying signals from receptors on the cell surface to target molecules inside the cell (*7*). There, the second messenger signaling cascade can alter gene expression and cellular function. In the mammalian SCN, several neurotransmitters, such as vasoactive intestinal peptide (VIP), arginine vasopressin, and gastrin-releasing peptide, are suggested to be involved in the SCN neuronal network (*8*–*10*). Receptors of these ligands are coupled with heterotrimeric GTP-binding proteins (G proteins) and second messenger signalings, such as cAMP and Ca^{2+}. In the SCN, pharmacological approaches imply that intracellular cAMP and Ca^{2+} are involved in the input and/or output of the molecular circadian clock in the circadian oscillations of the SCN (*11*, *12*). Cytosolic Ca^{2+} concentration shows robust circadian rhythms in individual SCN neurons, and the rhythms do not require intercellular communication through the neuronal network (*13*, *14*). Another study showed that blocking of intercellular communication slightly compromises Ca^{2+} rhythms in individual SCN cells (*15*). In contrast, disruption of *Bmal1* function results in loss of cytosolic Ca^{2+} rhythm (*15*, *16*). Although several roles of Ca^{2+} signaling in the SCN were reported, little is known about the circadian dynamics of intracellular cAMP and its functions in the SCN neuronal networks. In particular, the relationship between neuronal activity, neurotransmitters, intracellular cAMP/Ca^{2+}, and the molecular clock in the SCN is not clearly understood.

In the present study, we simultaneously visualized the circadian rhythms of intracellular cAMP and Ca^{2+} in the SCN using bioluminescence (Okiluc-aCT) and fluorescence (GCaMP6s) and found that cAMP rhythms were driven by neuronal networks. We also visualized neurotransmitter release using a genetically encoded G protein–coupled receptor (GPCR) activation–based (GRAB) sensor and found that cAMP rhythms in the SCN are regulated by VIP from the SCN and adenosine from outside the SCN. Last, we optically manipulated intracellular cAMP using a *Beggiatoa* photoactivatable adenylyl cyclase (bPAC) and found that the manipulation of intracellular cAMP shifted circadian molecular rhythms in the SCN and behavioral rhythms. Our findings provide notable insights into the dynamics of intracellular cAMP in the central circadian clock neurons.

[1]Department of Neuroscience II, Research Institute of Environmental Medicine, Nagoya University, Furo-cho, Chikusa-ku, Nagoya 464-8601, Japan. [2]Department of Neural Regulation, Nagoya University Graduate School of Medicine, Nagoya 466-8550, Japan. [3]State Key Laboratory of Membrane Biology, Peking University School of Life Sciences, Beijing, China. [4]Institute of Transformative Bio-Molecules (WPI-ITbM), Nagoya University, Furo-cho, Chikusa-ku, Nagoya 464-8601, Japan. [5]Laboratory of Animal Integrative Physiology, Graduate School of Bioagricultural Sciences, Nagoya University, Furo-cho, Chikusa-ku, Nagoya 464-8601, Japan. [6]Department of Biological Sciences, School of Science, The University of Tokyo, Hongo 7-3-1, Bunkyo-ku, Tokyo 113-0033, Japan. [7]Chinese Institute for Brain Research (CIBR), Beijing, 102206, China. [8]Advanced Optics and Biological Engineering, Evident Corporation, Tokyo, Japan.
*Corresponding author. Email: dai-ono@riem.nagoya-u.ac.jp

RESULTS

Time-lapse imaging of intracellular cAMP and Ca^{2+} in the SCN slice

Previously, we developed Okiluc-CaM, which is a split-type bioluminescent Ca^{2+} probe (*17*). To measure intracellular cAMP concentration using bioluminescence proteins, we developed an Okiluc-based cAMP probe (Okiluc-aCT; Fig. 1A). The wavelength of maximum bioluminescence of Okiluc-aCT was approximately 610 to 620 nm with D-luciferin application (fig. S1A). The brightness of Okiluc-aCT was approximately six times higher than that of the North American firefly luciferase–based cAMP probe (*18*). To evaluate the functions of Okiluc-aCT, we transfected Okiluc-aCT into human embryonic kidney (HEK) cells and measured bioluminescence using a photomultiplier tube (PMT) as previously reported (*19*). The application of forskolin significantly increased the bioluminescence intensity in a dose-dependent manner, indicating that the bioluminescence intensity of Okiluc-aCT reflects intracellular cAMP concentration (fig. S1, B to D).

To perform time-lapse recordings of intracellular cAMP in the SCN, we prepared SCN slices from wild-type mice, infected them with adeno-associated virus (AAV)- human synapsin1 promoter (hSyn)-Okiluc-aCT, and then measured bioluminescence using a PMT. We observed robust circadian cAMP rhythms in the SCN, and the application of forskolin increased the intensity of bioluminescence (fig. S1, E and F). These results indicate that Okiluc-aCT can be used to analyze the circadian dynamics of intracellular cAMP in the SCN.

It is suggested that intracellular cAMP and Ca^{2+} rhythms are coupled with the TTFL (*20*). To monitor the spatiotemporal patterns of cAMP and Ca^{2+} rhythms in the SCN, we infected the SCN slices with AAV-hSyn-Okiluc-aCT and AAV-hSyn-GCaMP6s (Ca^{2+} fluorescence indicator) and simultaneously measured bioluminescence and fluorescence (Fig. 1, B to D). We observed robust circadian rhythms in Okiluc-aCT (referred to as cAMP) and GCaMP6s (referred to as Ca^{2+}) signals in the SCN, and no phase difference was found between the two rhythms when compared across the SCN (Fig. 1, D and E). We then analyzed the circadian rhythms of cAMP and Ca^{2+} in the SCN at the pixel level using a cosine curve fitting method (*21*). Ca^{2+} rhythms in the SCN showed wave-like patterns, and the peak phase of Ca^{2+} rhythms in the dorsal and ventral SCN was significantly different as compared with that of cAMP rhythms (Fig. 1E and movie S1). cAMP showed robust circadian rhythms in the SCN, but clear wave-like patterns were not observed, indicating that the spatiotemporal patterns of the two rhythms were different (movie S1). The normalized synchrony (mean vector, r) was not different between cAMP and Ca^{2+} rhythms when comparing the whole SCN, but they were significantly different when comparing the dorsal, middle, and ventral SCN (Fig. 1F). The application of forskolin reduced the amplitude of Ca^{2+} rhythms but did not change Ca^{2+} levels in the SCN. However, forskolin application significantly increased cAMP levels in the SCN (fig. S1I). These results suggest that intracellular cAMP and Ca^{2+} show circadian rhythms but

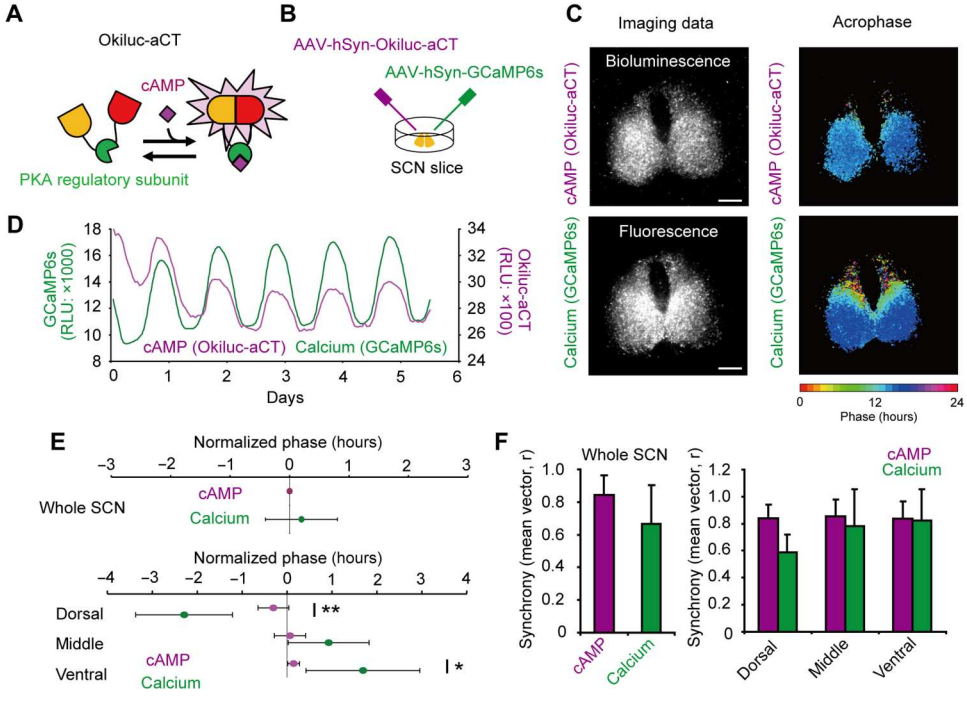

Fig. 1. Time-lapse imaging of intracellular cAMP and Ca^{2+} in the SCN. (**A** and **B**) Schematic drawing of the bioluminescence cAMP probe, Okiluc-aCT, and the viral infection of the SCN slice. PKA, protein kinase A. (**C**) Representative examples of bioluminescence (Okiluc-aCT) and fluorescence (GCaMP6s) images of the SCN slice and acrophase map calculated from the time series data. (**D**) Circadian cAMP (purple) and Ca^{2+} (green) rhythms in the SCN slice. (**E**) Mean acrophase of cAMP and Ca^{2+} rhythms in the SCN slice ($n = 4$). Phase 0 indicates mean acrophase of cAMP rhythms obtained from the whole SCN slice [$^{**}P < 0.01$ and $^{*}P < 0.05$, two-way repeated measures analysis of variance (ANOVA) followed by Bonferroni's multiple comparisons test]. (**F**) For cAMP rhythms and for Ca^{2+} rhythms, the degree of synchrony within the slice at the pixel level was measured by the mean vector length from Rayleigh plots (two-way repeated measures ANOVA: region × probe interaction, $P = 0.0407$). Data are shown as means ± SD. Scale bars, 200 μm. Bioluminescence intensity was expressed as relative light units (RLU).

might have different functions for the circadian rhythms in the SCN.

Circadian cAMP rhythms in the SCN are driven by action potential–dependent mechanisms

Cellular circadian rhythms in the SCN are reinforced and synchronized by intercellular coupling within the neuronal network, which is an important function for stabilizing circadian rhythms (*5*, *6*). It is suggested that cAMP and Ca^{2+} signaling work as mediators of cellular coupling and/or circadian oscillation in the SCN (*11*, *12*, *20*). To investigate the contribution of the neuronal network to the intracellular cAMP and Ca^{2+} rhythms of the SCN, we used a voltage-gated Na^{+} channel blocker, tetrodotoxin (TTX), which inhibits action potentials, resulting in the blocking of cellular coupling in the SCN (*4*, *22*). TTX application reduced the amplitude of cAMP and Ca^{2+} rhythms, and the amplitude of cAMP rhythms was significantly smaller than that of the Ca^{2+} rhythms in the SCN during TTX application (Fig. 2, A and C). Then, circadian rhythms in the SCN were analyzed at the pixel level. Application of TTX to the cultured SCN resulted in a slight decrease in the percent rhythm value (which indicates the prominence of the rhythm) of circadian Ca^{2+} rhythms but resulted in a significant decrease in the percent rhythm value of circadian cAMP rhythms at a significant level ($P = 0.01$; Fig. 2D and movie S2). Furthermore, synchrony of cellular cAMP rhythms was significantly attenuated by TTX application (Fig. 2E). The concentration of both cAMP and Ca^{2+} in SCN neurons during TTX application also decreased (Fig. 2F). These results suggest that intracellular cAMP rhythms in the SCN are driven by action potential–dependent mechanisms.

Circadian cAMP rhythms in the SCN are driven by rhythmic VIP release from the SCN

Attenuation of circadian rhythmicity in the SCN during TTX application was more evident in cAMP compared to Ca^{2+} (Fig. 2, C to F), suggesting that action potentials play a more important role in coordinating cAMP rhythms than Ca^{2+} rhythms. TTX could inhibit neurotransmitter release, which results in the desynchronization of cellular rhythms in the SCN. VIP is expressed in the SCN (*23*), which is important for cellular coupling (*8*, *10*). Furthermore, VIP receptor 2 (VPAC2) is a GPCR that activates adenylate cyclase and may be coupled to cAMP rhythms in the SCN (*24*). Therefore, we hypothesized that rhythmic VIP release is crucial for intracellular cAMP rhythms in the SCN. To understand the relationship between cAMP/Ca^{2+} rhythms and VIP in the SCN, we applied an excessive amount of VIP (1 μM) to the culture medium to block the VIP-related neuronal network and measured cAMP and Ca^{2+} rhythms in the SCN slice (Fig. 3A). As predicted, the amplitude of cAMP rhythms was significantly smaller than that of the Ca^{2+} rhythms in the SCN during VIP application (Fig. 3, A and C). Furthermore, the application of VIP increased cAMP concentration

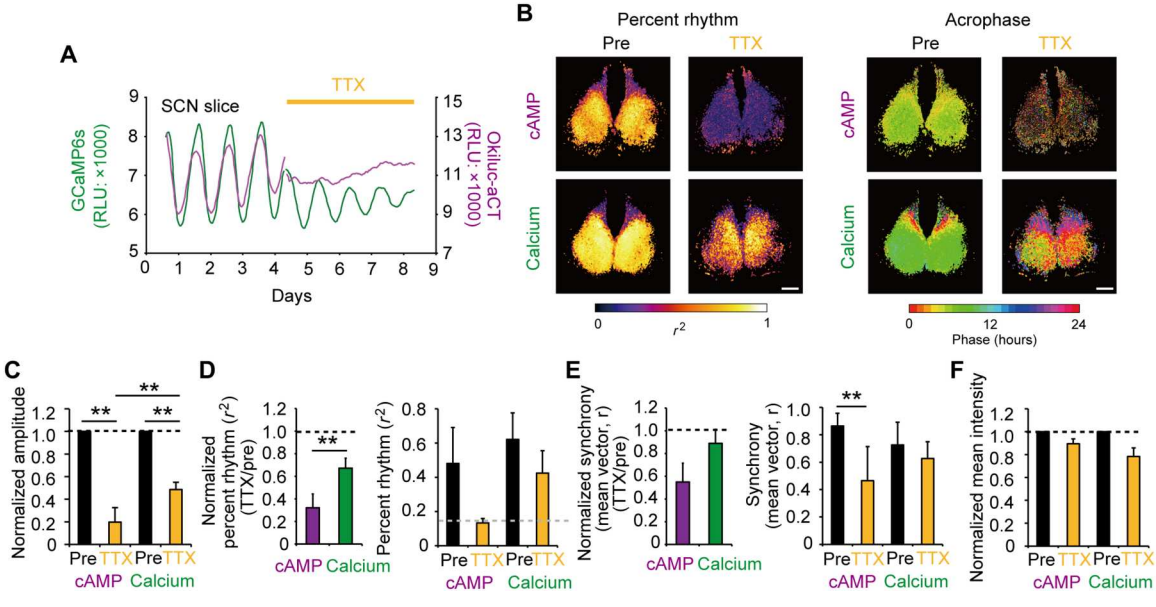

Fig. 2. Circadian cAMP rhythms in the SCN are driven by action potential–dependent mechanisms. (**A**) Representative example of circadian cAMP and Ca^{2+} rhythms in the SCN slice during TTX (0.5 μM) application. (**B**) Percent rhythm and acrophase map of cAMP and Ca^{2+} rhythms in the SCN slice before and during TTX application. Percent rhythm refers to rhythm prominence, defined as the percentage of the variance accounted for by the fitted cosine model, which corresponds to the coefficient of determination r^2 in the regression analysis (*56*). (**C**) Normalized amplitude of cAMP and Ca^{2+} rhythms in the SCN slice. The amplitude before TTX application was normalized as 1.0 ($n = 6$; $^{**}P < 0.01$, two-way repeated measures ANOVA followed by Bonferroni's multiple comparisons test). (**D**) Normalized (left) and mean value (right) of percent rhythm of cAMP and Ca^{2+} rhythms in the SCN before and during TTX application. Percent rhythm before TTX application was normalized as 1.0 ($^{**}P < 0.01$, paired *t*-test). The dotted gray line in the right panel indicates the significance level ($P = 0.01$). TTX application attenuated percent rhythm near the level of significance (two-way repeated measures ANOVA: main effect of the drug, $P < 0.001$; main effect of the probe, $P = 0.0159$). (**E**) For cAMP rhythms and for Ca^{2+} rhythms, the degree of synchrony within the slice at the pixel level was measured by the mean vector length from Rayleigh plots before and during the TTX application. Normalized (left) and mean value (right) of synchrony of cAMP and Ca^{2+} rhythms in the SCN before and during TTX application ($^{**}P < 0.01$, two-way repeated measures ANOVA followed by Bonferroni's multiple comparisons test). (**F**) Normalized mean intensity of Okiluc-aCT and GCaMP6s in the SCN 24 hours before and after TTX application (two-way repeated measures ANOVA: main effect of the drug, $P < 0.001$). Data are shown as means ± SD. Scale bars, 200 μm.

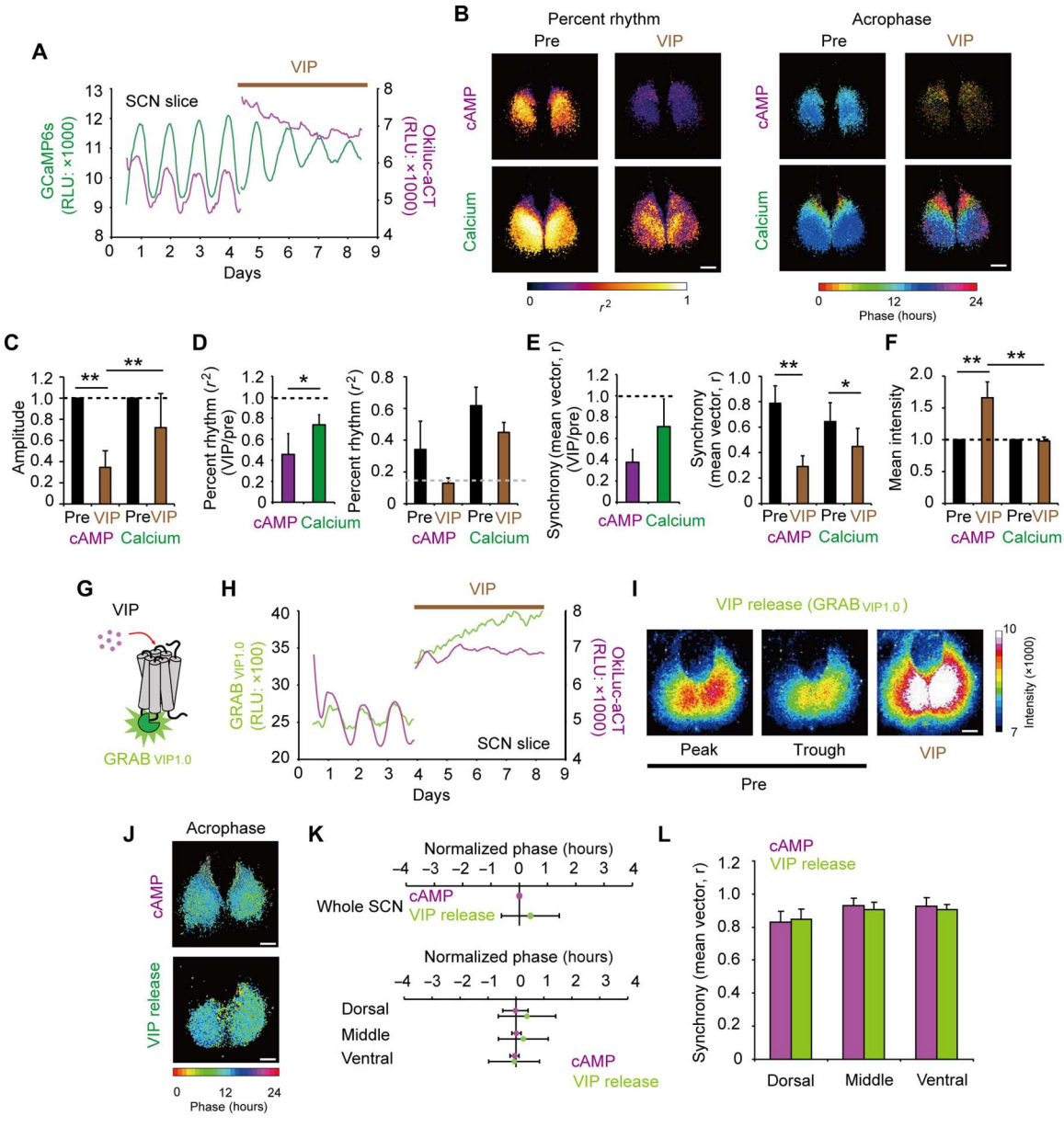

Fig. 3. Circadian cAMP rhythms in the SCN are driven by rhythmic VIP release from the SCN. (**A**) Representative example of circadian cAMP and Ca^{2+} rhythms in the SCN slice during VIP (1 μM) application. (**B**) Percent rhythm and acrophase map of cAMP and Ca^{2+} rhythms in the SCN slice before and during VIP application. (**C**) Normalized amplitude of cAMP and Ca^{2+} rhythms in the SCN slice before and during VIP application ($n = 5$; $^{**}P < 0.01$, two-way repeated measures ANOVA followed by Bonferroni's multiple comparisons test). (**D**) Normalized (left) and mean value (right) of percent rhythm of cAMP and Ca^{2+} rhythms in the SCN before and during VIP application ($^{**}P < 0.01$, paired *t*-test). The dotted gray line in the right panel indicates the significance level ($P = 0.01$). VIP application attenuated percent rhythm value near the level of significance (two-way repeated measures ANOVA: main effect of the drug, $P = 0.0011$; main effect of the probe, $P = 0.001$). (**E**) Normalized (left) and mean value (right) of synchrony of cAMP and Ca^{2+} rhythms in the SCN before and during VIP application ($^{**}P < 0.01$ and $^{*}P < 0.05$, two-way repeated measures ANOVA followed by Bonferroni's multiple comparisons test). (**F**) Normalized mean intensity of Okiluc-aCT and GCaMP6s in the SCN 24 hours before and after VIP application ($^{**}P < 0.01$, two-way repeated measures ANOVA followed by Bonferroni's multiple comparisons test). (**G**) Schematic drawing of $GRAB_{VIP1.0}$ sensor. (**H**) Representative example of circadian cAMP and VIP release rhythms in the SCN slice. (**I**) Pseudo color maps of fluorescence intensity obtained from $GRAB_{VIP1.0}$ sensor. (**J**) Representative example of acrophase of circadian cAMP and VIP release rhythm in the SCN slice. (**K**) Acrophase of cAMP and VIP release rhythms in the SCN slice ($n = 4$). (**L**) The degree of synchrony within the slice at the pixel level. Data are shown as means ± SD. Scale bars, 200 μm.

and decreased the percent rhythm value of cAMP rhythm at a significant level (P = 0.01; Fig. 3, A, B, D, and F, and movie S3). However, the VIP application did not change the level of Ca^{2+} concentration and only slightly attenuated the percent rhythm value (Fig. 3, D and F). Synchrony of circadian rhythms was significantly attenuated in cAMP and Ca^{2+} rhythms in the SCN (Fig. 3E). These results suggest that the circadian rhythms of cAMP may be mainly regulated by VIP release from the SCN.

If VIP release is crucial for cAMP rhythms in the SCN, then its release should show circadian oscillations. To determine whether VIP is rhythmically released in the SCN, we introduced a genetically encoded GRAB VIP sensor ($GRAB_{VIP1.0}$) (*25*). Circularly permutated green fluorescent protein was inserted into VPAC2, and the sensor showed fluorescent changes depending on the extracellular VIP concentration, which allowed us to monitor VIP release or VIP binding to the receptors (Fig. 3G). We infected the cultured SCN slices with AAV-hSyn-$GRAB_{VIP1.0}$ and AAV-hSyn-Okiluc-aCT and simultaneously measured VIP release and cAMP rhythms. We observed circadian rhythms of VIP release in the SCN, and the peak phase of circadian VIP release was the same as that of cAMP rhythms (Fig. 3, H, J, and K, and movie S4). Furthermore, no phase gradient was observed in the VIP release rhythms, which had the same patterns of cAMP rhythms in the SCN (Fig. 3, J and K). Excessive VIP application increased the intensity of Okiluc-aCT and $GRAB_{VIP1.0}$ in the SCN. Even when only $GRAB_{VIP1.0}$ was expressed in the SCN, it exhibited circadian rhythms (fig. S2). These results suggest that intracellular cAMP rhythms may be regulated by the rhythmic release of VIP in the SCN.

Neuronal activity is critical for VIP release in the SCN

Because intracellular cAMP rhythms in the SCN were not observed during TTX application and these rhythms were driven by the rhythmic release of VIP (Figs. 2 and 3), we hypothesized that the rhythmic release of VIP depends on neuronal activity in the SCN. To answer this, we measured VIP release and molecular oscillation in the SCN slice using $GRAB_{VIP1.0}$ and PERIOD2 (PER2)::LUC reporter (a fusion protein of PER2 and firefly luciferase), respectively, and applied TTX. The difference in the peak phases of these rhythms was 5.0 ± 0.8 hours (n = 4; Fig. 4A). As predicted, the amplitude of $GRAB_{VIP1.0}$ and PER2::LUC rhythms was decreased during TTX application (Fig. 4, A and C). The percent rhythm value of circadian rhythms of VIP release was decreased at a significant level during TTX application (P = 0.01; Fig. 4D and movie S5). Synchrony of circadian rhythms was attenuated in the $GRAB_{VIP1.0}$ and PER2::LUC rhythms in the SCN (Fig. 4E). TTX application to the cultured SCN decreased the PER2::LUC level (Fig. 4F). These results indicate that circadian rhythms of VIP release are driven by neuronal activity in the SCN.

Circadian cAMP dynamics in the SCN are modulated by VIP and adenosine

In the SCN, adenosine A2A receptors are expressed (*26*). These receptors are G_s-coupled GPCRs that have the potential to increase cytosolic cAMP concentration. To determine whether adenosine signaling changes cAMP rhythms in the SCN, we applied an adenosine agonist (IB-MECA) and measured cAMP and Ca^{2+} rhythms in the SCN. Application of IB-MECA (10 μM) significantly increased the amplitude of circadian cAMP rhythms (Fig. 5C), but the application also increased cytosolic cAMP concentration in the SCN (Fig. 5, A and F). Although a significant increase in cAMP by the adenosine agonist was observed, the robustness and synchrony of circadian cAMP rhythms were not affected (Fig. 5, D and E). This is due to the fact that under IB-MECA (10 μM) application, VIP is still rhythmically released (fig. S2). These results suggest that cytosolic cAMP concentration in the SCN is regulated by VIP and adenosine.

To further understand the functional role of SCN-secreted VIP and adenosine in the circadian rhythms of intracellular cAMP, we introduced VPAC2 and adenosine A2A receptor antagonists. We measured cAMP rhythms in the SCN using Okiluc-aCT and applied a VPAC2 antagonist (PG99-465) or an adenosine A2A receptor antagonist (ZM241385). PG99-465 (1 μM) application attenuated the amplitude of cAMP rhythms in the SCN; in contrast, ZM241385 (100 nM and 5 μM) did not change the amplitude of cAMP rhythms as compared with the dimethyl sulfoxide (DMSO) control (Fig. 5, G and H). Furthermore, PG99-465 (1 μM) application decreased the amplitude of circadian PER2::LUC rhythms at the SCN slice level and desynchronized cellular circadian rhythms in the SCN (fig. S3), which are similar results to that of VIP-deficient SCN. We also confirmed that the cAMP level in the SCN was increased depending on VIP concentration (fig. S1, G and H). These results suggest that the main contribution of intracellular cAMP rhythms in the SCN is the rhythmic release of VIP from the SCN and adenosine from outside the SCN could also influence the intracellular cAMP concentration.

Optical manipulation of intracellular cAMP shifts circadian PER2::LUC rhythms in the SCN slice

Intracellular cAMP rhythms were attenuated by the application of TTX and excessive VIP (Figs. 2 and 3). Furthermore, it is suggested that cAMP functions as an input factor for molecular oscillations in the SCN (*11*, *12*). If this is true, manipulation of cAMP could shift the circadian molecular rhythms in the SCN. To clarify this, we introduced a bPAC, which translates a blue light signal into the production of cAMP (*27*). First, we prepared SCN slices from glutamate decarboxylase (GAD67)-Cre mice and infected them with AAV-CMV-flex-bPAC-2A-mCherry and AAV-hSyn-Okiluc-aCT. Because almost all SCN neurons are GABAergic, we used GAD67-Cre mice. We confirmed that blue light stimulation (10 Hz; duration, 20 ms) significantly increased bioluminescence intensity in HEK cells and the SCN, indicating that blue light stimulation increases cAMP levels in the SCN (fig. S4). Next, to measure molecular circadian rhythms, we made SCN slices from GAD67-Cre or control mice with the PER2::LUC heterozygous reporter and then infected the SCN slice with AAV-hSyn-bPAC-2A-mCherry (Fig. 6, A and C). After recording PER2::LUC bioluminescence for several days, we flashed blue light (10 Hz) for 1 hour, and bioluminescence was measured again (Fig. 6B). Flashing blue light for 1 hour around circadian time (CT) 6 to 12 (CT12 is defined as the peak phase of the PER2::LUC rhythm in the SCN) caused phase delay shifts of PER2::LUC rhythms in the SCN of GAD67-Cre mice but not in the control mice (Fig. 6, D to F, and fig. S3). In addition, optical manipulation of cAMP in the SCN under VPAC2 antagonist application induced a large phase delay shift as compared with vehicle application (fig. S5B). We also checked the dose-dependent effects of light stimulation on the circadian PER2::LUC rhythms

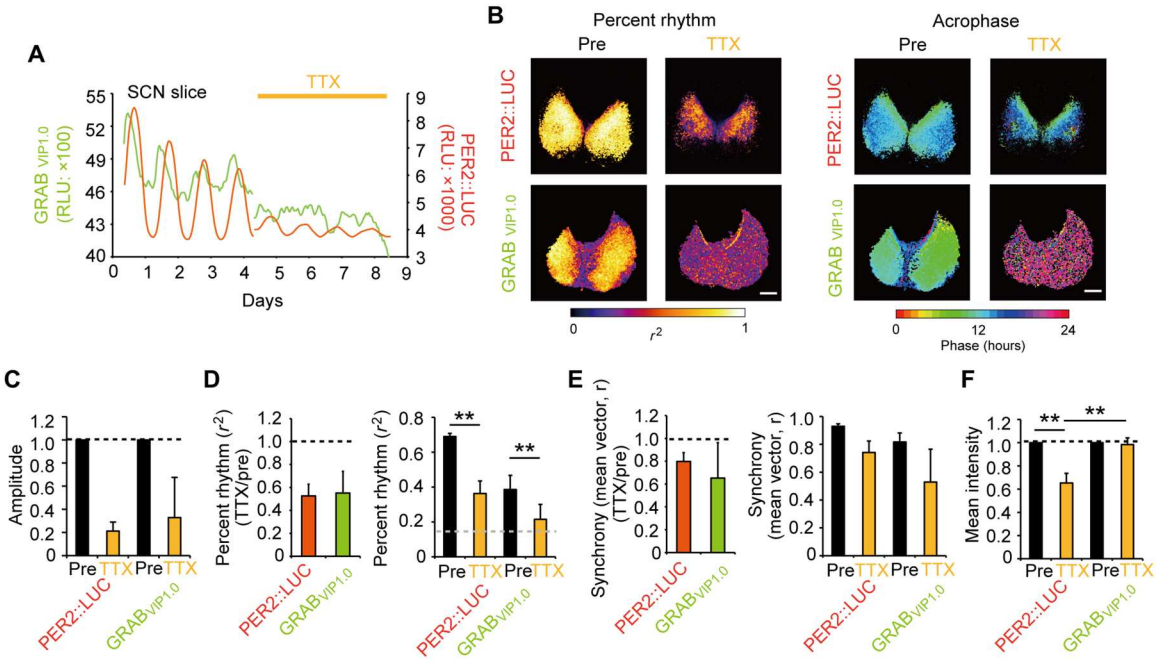

Fig. 4. Neuronal activity is critical for VIP release in the SCN. (**A**) Representative example of circadian VIP release and PER2::LUC rhythms in the SCN slice during TTX (0.5 μM) application. (**B**) Percent rhythm and acrophase map of VIP release and PER2::LUC rhythms in the SCN slice before and during TTX application. (**C**) Normalized amplitude of VIP release and PER2::LUC rhythms in the SCN slice before and during TTX application. The amplitude before TTX application was normalized as 1.0 ($n = 4$; two-way repeated measures ANOVA: main effect of the drug, $P = 0.0002$). (**D**) Normalized (left) and mean value (right) of percent rhythm of VIP release and PER2::LUC rhythms in the SCN before and during VIP application. Percent rhythm before VIP application was normalized as 1.0. The dotted gray line in the right panel indicates the significance level ($P = 0.01$). VIP application attenuated percent rhythm value near the level of significance (**$P < 0.01$, two-way repeated measures ANOVA followed by Bonferroni's multiple comparisons test). (**E**) Normalized (left) and mean value (right) of synchrony of VIP release and PER2::LUC rhythms in the SCN before and during VIP application (two-way repeated measures ANOVA: main effect of the drug, $P = 0.0113$; main effect of the probe, $P = 0.0431$). (**F**) Normalized mean intensity of $GRAB_{VIP1.0}$ and PER2::LUC in the SCN 24 hours before and after TTX application (**$P < 0.01$, two-way repeated measures ANOVA followed by Bonferroni's multiple comparisons test). Data are shown as means ± SD. Scale bars, 200 μm.

in the SCN (fig. S5C). These results indicate that phase-dependent manipulation of cAMP shifts circadian rhythms in the SCN.

Because intercellular coupling via VIP is critical for synchronizing rhythms of oscillators across the SCN, if the VIP-dependent network regulates cAMP rhythms in the SCN, then suppression of cAMP should affect circadian molecular rhythms in the SCN but not in culture cell lines that lack VIP-dependent coupling. To assess this possibility, we added the adenylate cyclase inhibitor (MDL12330A) into the culture medium and measured PER2::LUC rhythms in the SCN. We observed that MDL12330A (5 μM) application significantly attenuated the amplitude of PER2::LUC circadian rhythms in the SCN, which was consistent with previous reports (fig. S6A) (*12*, *21*). However, MDL12330A (5 μM) application did not change the amplitude of circadian rhythms in *Per2-luc* of U2OS cells (fig. S6B). Together, these results indicate that intracellular cAMP rhythms driven by rhythmic VIP release in the SCN may modulate circadian molecular rhythms.

Optical manipulation of intracellular cAMP shifts circadian behavioral rhythms

Last, to characterize the role of cAMP in vivo, we measured circadian behavioral rhythms in constant darkness (DD) while optogenetically manipulating cAMP levels in the SCN. We injected AAV with Cre-dependent expression of bPAC or tdTomato into the SCN of GAD67-Cre mice and inserted an optical fiber just above the SCN (Fig. 7, A and C). Locomotor activity was measured using an infrared sensor as previously described (*21*). After housing in DD for approximately 10 days, we flashed blue light (10 Hz) for 1 hour every 24 hours. Behavioral rhythms of bPAC-expressing GAD67-Cre mice were shifted by flashing blue light (Fig. 7B and fig. S5A). On the other hand, control mice in which bPAC expression failed continued to free-run independent of flashing blue light (Fig. 7 and fig. S5, B to D). The circadian period during blue light stimulation was significantly different between pre- and post-flashing in bPAC-expressing GAD67-Cre mice, but it was not different in the control mice (Fig. 7D). These results indicate that optical manipulation of intracellular cAMP shifts circadian behavioral rhythms.

DISCUSSION

In this study, we used a cAMP bioluminescence probe combined with $GRAB_{VIP1.0}$ sensor or bPAC and found that (i) the circadian rhythms of intracellular cAMP in the SCN were driven by neuronal activity, (ii) neuronal activity regulated rhythmic VIP release, (iii) circadian rhythms of VIP release further regulated cAMP rhythms in the SCN, (iv) VIP from the SCN and adenosine from outside the SCN might contribute to cAMP rhythms in the SCN, and (v) optical manipulation of cAMP in the SCN shifted the molecular circadian rhythms in the SCN and locomotor activity

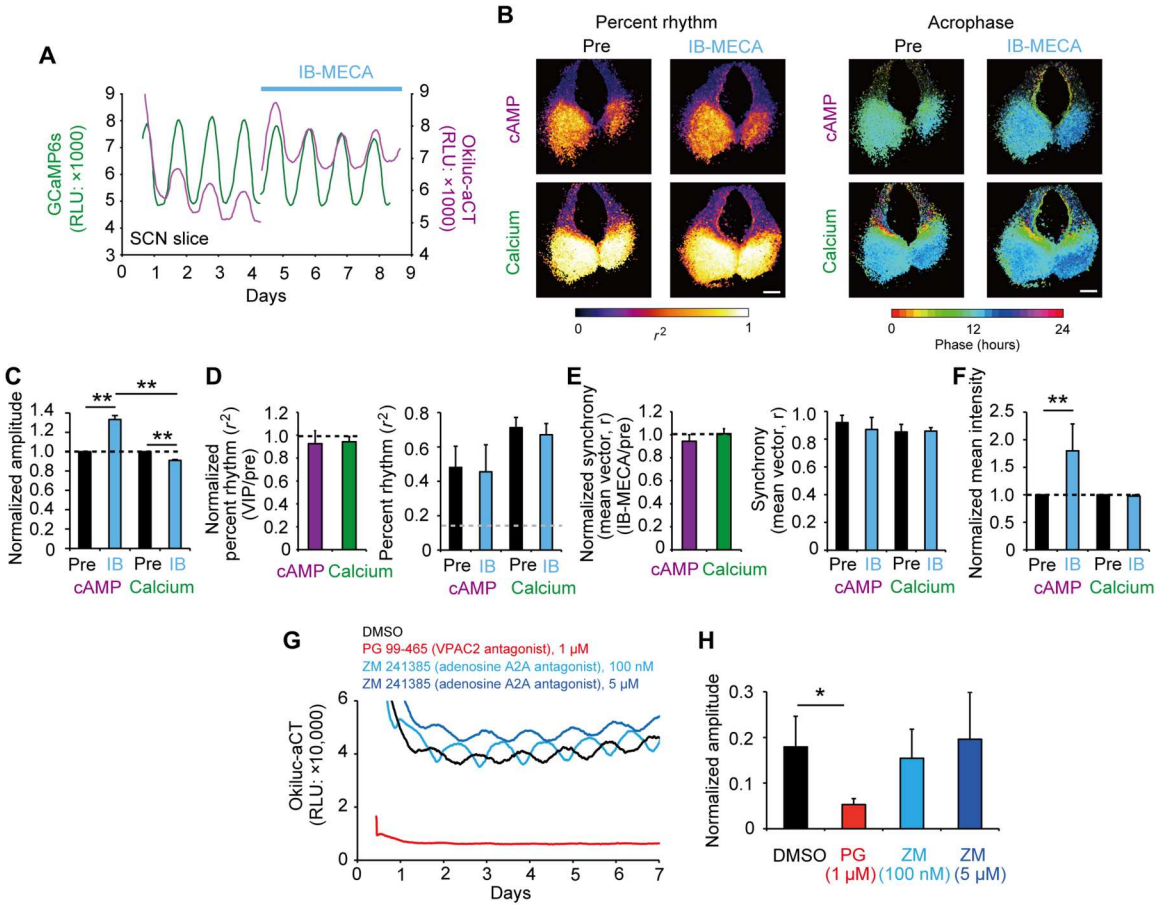

Fig. 5. Circadian cAMP dynamics in the SCN are modulated by VIP and adenosine. (**A**) Representative example of circadian cAMP and Ca^{2+} rhythms in the SCN slice during adenosine agonist (IB-MECA, 10 μM) application. (**B**) Percent rhythm and acrophase map of cAMP and Ca^{2+} rhythms in the SCN slice before and during IB-MECA application. (**C**) Normalized amplitude of cAMP and Ca^{2+} rhythms in the SCN slice. The amplitude before IB-MECA application was normalized as 1.0 ($n = 5$; $^{**}P < 0.01$, two-way repeated measures ANOVA followed by Bonferroni's multiple comparisons test). (**D**) Normalized (left) and mean value (right) of percent rhythm of cAMP and Ca^{2+} rhythms in the SCN before and during IB-MECA application. Percent rhythm before IB-MECA application was normalized as 1.0. The dotted gray line in the right panel indicates the significance level ($P = 0.01$) (two-way repeated measures ANOVA: main effect of the drug, $P = 0.0294$; main effect of the probe, $P = 0.0108$). (**E**) Normalized (left) and mean value (right) of synchrony of cAMP and Ca^{2+} rhythms in the SCN before and during IB-MECA application. (**F**) Normalized mean intensity of Okiluc-aCT and GCaMP6s in the SCN 24 hours before and after IB-MECA application ($^{**}P < 0.01$, two-way repeated measures ANOVA followed by Bonferroni's multiple comparisons test). (**G**) Representative examples of cAMP rhythms in the SCN slice during DMSO (black, $n = 5$), VPAC2 antagonist (red, $n = 4$; PG 99 to 465, 1 μM), and adenosine A2A antagonist (light blue, $n = 4$; ZM241385, 100 nM; dark blue, $n = 4$; ZM241385, 5 μM) application. (**H**) Mean relative amplitude of cAMP rhythms during DMSO or antagonist application ($^{*}P < 0.05$, one-way ANOVA followed by Dunnett's multiple comparisons test). Data are shown as means ± SD. Scale bars, 200 μm.

rhythms. These results demonstrate that intracellular cAMP in the SCN is a key mediator in the circadian neuronal network (fig. S8).

The existence of intracellular cAMP rhythms in the SCN was reported using intermittent tissue sampling of the SCN (*12*, *28*, *29*), which lacked precise spatiotemporal information on cAMP rhythms in the SCN. In the present study, we successfully visualized intracellular cAMP rhythms together with Ca^{2+} rhythms in the SCN and found that circadian cAMP and Ca^{2+} rhythms showed different spatiotemporal patterns. These results suggest that circadian cAMP and Ca^{2+} rhythms play different roles in the SCN. TTX application seemed to attenuate circadian Ca^{2+} rhythmicity in the SCN (Fig. 2), which is consistent with previous work (*15*), suggesting that circadian Ca^{2+} rhythms are regulated by intracellular oscillatory mechanisms and neuronal networks. Recently, Morioka *et al.* (*30*) reported that the knockdown of a mitochondrial cation antiporter (Leucine zipper-EF-hand-containing transmembrane protein 1: LETM1) in the SCN deteriorated circadian molecular and Ca^{2+} rhythms, suggesting that Ca^{2+} rhythms in SCN neurons could be associated with mitochondrial ion transport. In contrast, TTX application significantly attenuated the circadian rhythmicity of cAMP (Fig. 2) and the cAMP response element (CRE) activity in SCN neurons (*31*), indicating that intercellular communication in the SCN neuronal network is critical for intracellular cAMP rhythms in the SCN.

Using the GRAB sensor, we first visualized the spatiotemporal patterns of circadian VIP release in the SCN. This result is consistent with those of previous studies that lacked spatiotemporal information (*32*, *33*). Here, we found that the circadian phase of VIP release and cAMP rhythms were similar in the SCN, and the application of VIP increased cAMP levels but did not increase Ca^{2+} levels (Fig. 3). Furthermore, circadian Ca^{2+} rhythms, but not cAMP rhythms, were observed during VIP administration. The degree of

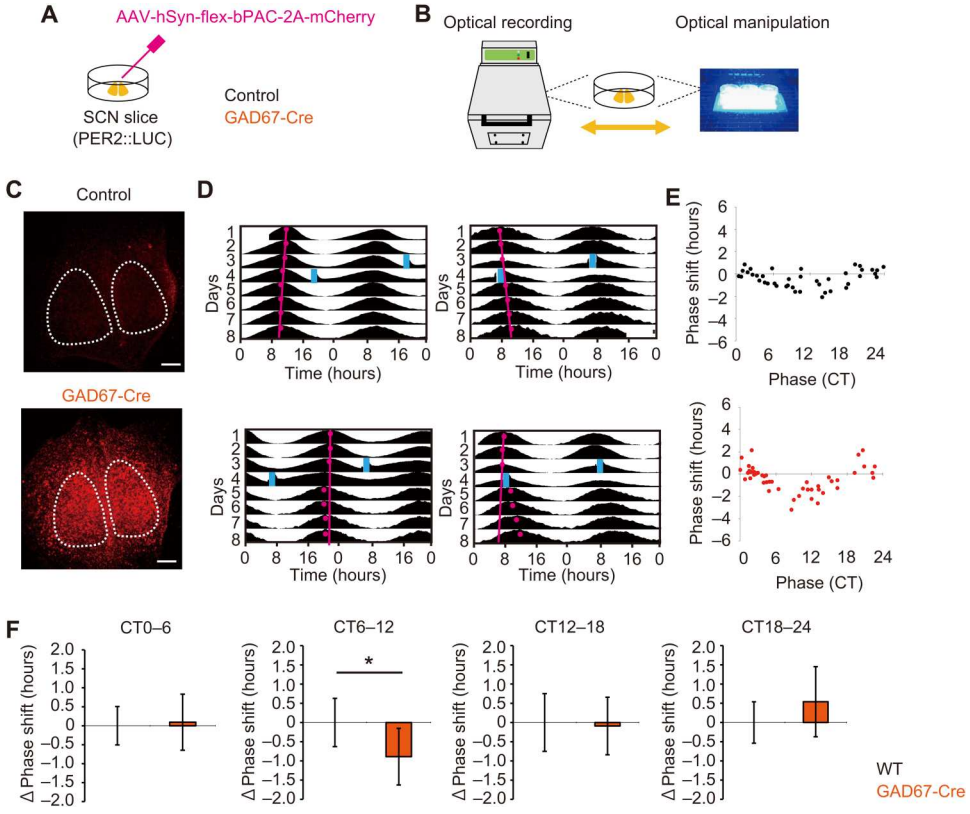

Fig. 6. Optical manipulation of intracellular cAMP shifts circadian PER2::LUC rhythms in the SCN slice. (**A** and **B**) Schematic drawing of viral infection of SCN slices from PER2::LUC reporter mice and experimental scheme of optical recording and manipulation. (**C**) Representative examples of fluorescence images in the SCN slices of control or GAD67-Cre mice. (**D**) Double-plotted PER2::LUC rhythms in the SCN. Blue rectangles indicate the timing of the flashing blue light (10 Hz, 1 hour). Acrophases and regression lines obtained from PER2::LUC rhythms before blue light stimulation are shown by magenta dots and a line, respectively. (**E**) The phase response curve of PER2::LUC rhythms in control and GAD67-Cre SCN. The peak phase of PER2::LUC was defined as CT12. (**F**) Quantified data of Δ phase shift (0 defined as the mean phase shift of control) of PER2::LUC rhythms (control: $n = 41$ trials from 16 SCN slices; GAD67-Cre: $n = 48$ trials from 17 SCN slices; $^*P < 0.05$, mixed-effects model with post hoc Sidak's multiple comparisons test). The presented data are quantification of the phase shift separated by the time in the circadian phase at which the pulse of bPAC was provided. Data are shown as means ± SD. Scale bars, 200 μm. Wild type, WT.

synchrony of Ca^{2+} rhythms within the slice at the pixel level was attenuated by the VIP application. These results suggest that the rhythmic release of VIP from the SCN driven by neuronal activity is critical for the synchronization of cellular circadian Ca^{2+} rhythms, and it is crucial for the circadian rhythmicity of cAMP in the SCN cells.

We also found that intracellular cAMP levels were regulated by adenosine. This regulation may be due to adenosine A2A G_s-coupled receptors (*34*), and the application of an adenosine agonist increased cAMP concentration in the SCN (Fig. 5). However, endogenous adenosine within the SCN slice may not appear to play a role in driving cAMP rhythms because pharmacological suppression of adenosine A2A receptors had no effect (Fig. 5). Inhibition of adenosine signaling suppresses light-induced phase shifts of behavioral rhythms (*26*), and caffeine works as an antagonist of adenosine A2A receptors (*35*). Furthermore, the adenosine concentration in the SCN obtained from in vivo sampling has shown circadian rhythms in which the peak phase was located during the day (*26*). Thus, the rhythmic release of VIP from the SCN and adenosine release outside the SCN could contribute to intracellular cAMP rhythm in the SCN in vivo.

VIP treatment of SCN slices around CT10 causes phase delay shifts in circadian PER2::LUC rhythms (*24*). Furthermore, optical stimulation of VIP neurons using channelrhodopsin-2 (ChR2) also induces phase delay shifts in circadian rhythms in the SCN (*36*). These delays associated with VIP or VIP neuronal stimulation may depend on the induction of intracellular cAMP in the SCN slice because optogenetic activation of cAMP concentration in the SCN showed similar phase shifts to PER2::LUC rhythms (Fig. 6). However, the cAMP analogs only induced phase advance shifts in circadian firing rhythms in the SCN (*37*). This discrepancy may be due to differences in overt rhythm recording methods. It is reported that clock gene and firing rhythms in the SCN exhibit different rhythms (*38*, *39*). VIP application increased cAMP levels in the SCN, but it did not increase intracellular Ca^{2+} levels, suggesting that VIP release directly regulates intracellular cAMP rhythms, but not Ca^{2+} rhythms, in the SCN (Fig. 3).

Although VIP and adenosine may regulate intracellular cAMP concentration, other factors also have the potential to modulate cAMP rhythms in the SCN. For instance, regulators of G protein signaling 16 (*Rgs16*) or *Gpr176* have a role in the modulation of intracellular cAMP rhythms, and Rgs16 deficiency impairs spatiotemporal patterns of *Per1-luc* expression rhythms in the SCN (*28*, *40*).

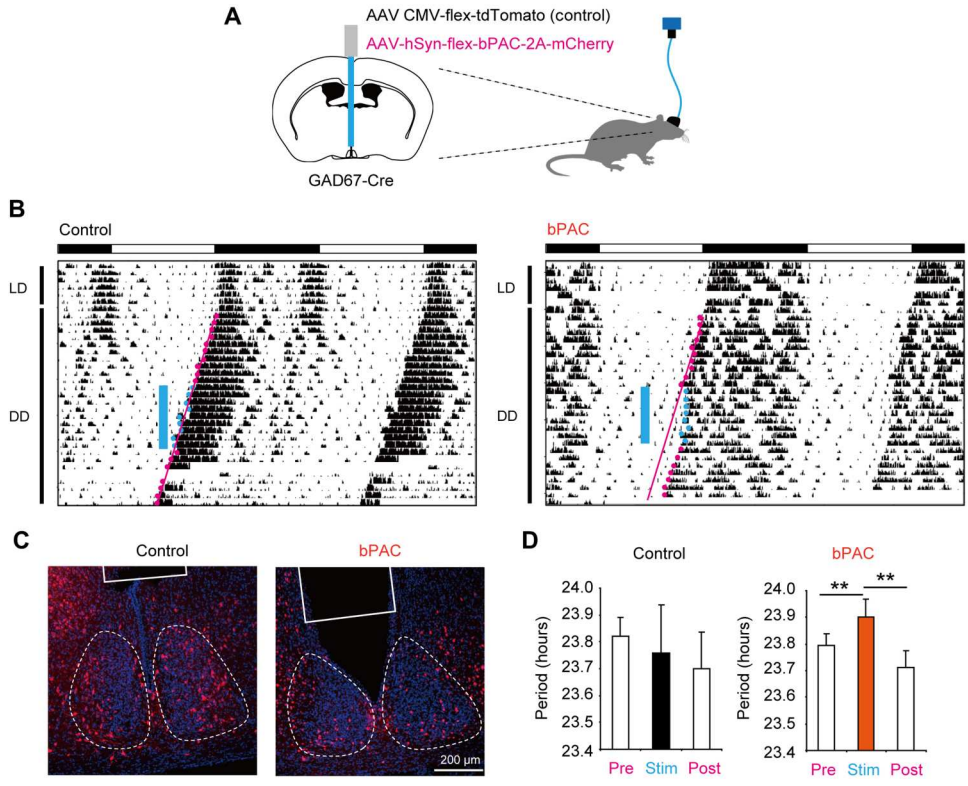

Fig. 7. Optical manipulation of intracellular cAMP shifts circadian behavioral rhythms. (**A**) Schematic drawing of the experimental setup of in vivo optogenetics. AAV was injected into the SCN, and an optical fiber was inserted just above the SCN. (**B**) Representative examples of double-plotted actogram of control and bPAC-expressed mice under light-dark (LD) and DD conditions. The blue rectangle indicates the timing of blue light stimulation (10 Hz, 1 hour/day). Activity onset is plotted as a colored circle (magenta, pre and post; blue, during light stimulation), and the regression lines (magenta) are fit through locomotor activity onsets before blue light stimulation and extrapolated thereafter. (**C**) Fluorescence images of the SCN (red, mCherry or tdTomato; blue, 4′,6-diamidino-2-phenylindole). Solid lines indicate an estimated trace of an optical fiber. Broken lines indicate an estimated border of the SCN. (**D**) Quantified data of circadian period before, during, and after blue light stimulation (control, $n = 6$; bPAC, $n = 7$; $^{**}P < 0.01$, one-way repeated measures ANOVA with post hoc Tukey-Kramer test). Data are shown as means ± SD. Scale bars, 200 μm.

Furthermore, the *Cry* protein inhibits GPCR activity directly through interaction with Gsα (*41*). Thus, rhythmic changes in extra- and intracellular factors contribute to circadian cAMP rhythms in the SCN.

VIP-deficient mice show deteriorated circadian behavioral rhythms and desynchrony of cellular circadian rhythms in the SCN (*8*, *42*). We found that cAMP rhythms were regulated by the rhythmic release of VIP from the SCN, and optical manipulation of cAMP induced a phase shift of circadian rhythms of the SCN. Furthermore, we observed that optical manipulation of cAMP in the SCN induced a large phase shift under VPAC2 receptor antagonist application. Therefore, it would be possible to rescue the VIP defect in vivo using optical manipulation of cAMP in the SCN.

Increased cAMP levels facilitate the induction of the phosphorylated form of the transcription factor cAMP response element–binding protein (CREB), which binds the CRE located in the promoter region of *Per1* and *Per2* (*43*). CRE-mediated gene expression shows circadian rhythms in which the circadian peak phase is approximately CT12 (*44*). The CREB and CRE pathways are thought to be important pathways located downstream of cAMP rhythms (*31*). However, other input pathways are also suggested to be involved with the input pathway to the TTFL. For example, *Cry1* promoter–driven luciferase activity shows circadian rhythms in *Per1*/*Per2* null SCN with coculturing of the wild-type SCN (*45*), although the CRE sequence is not located in the *Cry1* promoter region. Therefore, CRE-dependent and CRE-independent input pathways from cAMP to TTFL may be involved in the intracellular mechanisms of the circadian rhythm.

Intracellular Ca^{2+} levels in the SCN were suppressed by the TTX application, but the circadian Ca^{2+} rhythm was sustained during the application. Furthermore, the VIP application did not change the Ca^{2+} level in the SCN (Figs. 2 and 3). These results suggest that circadian Ca^{2+} rhythms in the SCN are regulated by both the TTFL and membrane potential but are indirectly regulated by VIP release. Circadian rhythms of VIP release drive intracellular cAMP rhythms in the SCN, which can reset TTFL oscillations. TTFL then regulates intracellular Ca^{2+} levels via cellular organelles, such as the endoplasmic reticulum, mitochondria, and/or extracellular space. Intracellular Ca^{2+} rhythms are suggested to be regulated by TTFL (*16*). However, circadian Ca^{2+} rhythms are observed in the SCN even when functional TTFL is disrupted (*Cry1*/*Cry2*-deficient SCN) (*46*). In previous studies, several clock gene–deficient mice (*Cry1*/*Cry2*-, *Bmal1*-, or *Per1*/*Per2*-deficient mice) showed circadian rhythms in the SCN slice, although these mice demonstrated arrhythmic behavior (*9*, *19*, *45*, *47*). A circadian oscillatory mechanism without TTFL was found in cyanobacteria (*48*, *49*), and a similar mechanism has also been suggested to be involved in mammalian cells (*50*, *51*). Thus, it is plausible that intracellular

Ca^{2+} and/or cAMP are coupled with non-TTFL oscillatory mechanisms. Further research will uncover the mechanisms of circadian oscillation without TTFL and its relationship with cytosolic events in the SCN.

In the present study, we simultaneously measured the second messenger signaling of cAMP and Ca^{2+} in the SCN using bioluminescence and fluorescence, respectively. Because these second messenger signaling pathways regulate a variety of cellular functions, such as the formation of long-term potentiation in the hippocampus, the long-term imaging (more than 1 week) of cAMP and Ca^{2+} that we performed in this study would be applicable to many fields in biology.

In conclusion, intracellular cAMP rhythms in the SCN are regulated by VIP-dependent neuronal networks and other factors outside the SCN. The network-driven cAMP rhythm coordinates circadian molecular rhythm in the SCN and behavioral rhythm.

MATERIALS AND METHODS

Animals

We used wild-type, GAD67-Cre (*52*), or *Vgat*-internal ribosome entry site (IRES)-Cre (*53*) mice with C57BL/6J background. The circadian reporter system was introduced by breeding PER2::LUC mice, which carry a fusion protein of PER2 and firefly luciferase (*54*). Mice were bred and reared in the animal facility at Nagoya University, where environmental conditions were controlled (lights on, 0800 to 2000, ambient temperature, 23° ± 2°C; humidity, 60 ± 10%). Mice had free access to food pellets and water. Male and female mice were used in the experiments. The day of birth was designated as postnatal day 0. All experimental protocols were approved by the Institutional Animal Care and Use Committees of the Research Institute of Environmental Medicine, Nagoya University, Japan (approval #R210729 and #R210730).

Bioluminescent cAMP indicator gene construction

The cDNA of firefly luciferase derived from *Pyrocoelia matsumurai* (Oki) and *Stenocladius flavipennis* (SfRE) were gifts from K. Ogo (Olympus Corporation). Okiluc-aCT was created following a previously reported methodology (*17*). An N-terminal fragment of mouse protein kinase A regulatory subunit Ia gene (amino acid residues L141 to V381; aCT) was fused to the C-terminal half (residues T352 to M555) of SfRE luciferase and to the N-terminal half (residues M1 to D416) of Oki luciferase at the C terminus. For bacterial and mammalian expression, the Okiluc-aCT gene was subcloned into the Bam HI/Eco RI sites of pRSET-B and pcDNA3.1(+) to construct pRSET-Okiluc-aCT and pcDNA3.1(+)-Okiluc-aCT, respectively.

In vitro titration of bioluminescent indicators

Recombinant proteins were purified from bacteria transformed with pRSET-Okiluc-aCT plasmids using QIAexpressionist (QIAGEN), following the manufacturer's instructions as previously reported (*17*). The concentration of purified protein was determined using a Bio-Rad protein assay and diluted with a buffer consisting of 10 mM ethylene glycol-bis(2-aminoethylether)-N,N,N′,N′-tetraacetic acid (EGTA), 100 mM KCl, and 10 mM Mops (pH 7.2) to a concentration of 1 μg of protein/μl. Recombinant protein (1 μg) was mixed with a dilution series of cAMP in 50 μl of buffer and incubated for 10 min at room temperature (<24°C). Following incubation, 50 μl of the sample was added to 50 μl of luciferase assay reagent (Bright-Glo; Promega) solution and incubated further for 15 min at room temperature. Luminescence was measured using a Luminescencer JNR (ATTO Corporation, Tokyo, Japan). The data from four independent measurements were averaged using Microsoft Excel 2003 (Microsoft Corporation, Redmond, WA), and the results are expressed as means ± SD.

Preparation of SCN slice culture

To measure the circadian rhythms of the SCN, coronal slices (300 μm thick) were made with a tissue chopper (McIlwain) from neonatal mice at postnatal days 5 to 7, and the SCN area was dissected at the mid rostrocaudal region. A paired SCN was cultured on a Millicell-CM culture insert (Millipore Corporation) as described previously (*17*). Briefly, the slice was cultured at 36.5°C with 1.0 ml of Dulbecco's modified Eagle's medium (DMEM; Invitrogen) with 5% fetal bovine serum. Two to 4 days after preparation of the SCN slice, we applied AAV (0.5 to 1.0 μl; AAV-hSyn-Okiluc-aCT, 6.3×10^{12} genome copies/ml; AAVSyn-flex-bPAC-2A-Cherry, 4.8×10^{12} genome copies/ml) onto the surface of the cultured SCN slice. More than 15 days after the viral infection, we started recording.

Measurement of bioluminescence from U2OS cells

Real-time monitoring of gene expression rhythms in U2OS cells stably expressing *Per2*-luc reporter was performed (*55*). The cells were plated on 35-mm dishes (5×10^5 cells per dish) and cultured at 37°C under 5% CO_2 in a culture medium of DMEM (Sigma-Aldrich, catalog no. D5796) supplemented with 10% FBS (Biosera, FB-1290/500), penicillin (50 U/ml), and streptomycin (50 μg/ml). One day after plating, the cells were treated with 0.1 μM dexamethasone for 1 hour, and the medium was replaced with a recording medium (DMEM; Sigma-Aldrich, catalog no. D2902) supplemented with 10% FBS, glucose (3.5 mg/ml), penicillin (25 U/ml), streptomycin (25 μg/ml), 0.1 mM luciferin, and 10 mM Hepes-NaOH (pH 7.0). The bioluminescence signals were continually recorded once per 10 min by a dish-type bioluminescence detector LumiCycle (Actimetrics) for 6 days as previously reported (*55*).

Measurement of bioluminescence and/or fluorescence on the SCN slice

To measure bioluminescence at the tissue level, we used a PMT equipped with a photon-counting device (Kronos, ATTO). The intensity of bioluminescence was recorded every 10 min with an exposure time of 1 min. D-Luciferase K (0.1 mM) was added to the culture medium. For the measurement of spatiotemporal patterns of circadian rhythms in the SCN, we used a microscope (ECLIPSE 80i or ECLIPSE Ni-U, Nikon) equipped with an electron-multiplying charge coupled device (EM-CCD) camera (ImagEM, Hamamatsu Photonics). Bioluminescence was measured without any optical filters, and the fluorescent calcium sensor (GCaMP6s) was excited at cyan color (470/40 nm) with a light-emitting diode (LED) light source (RETRA Light Engine; Lumencor, X-Cite 120; Excelitas Technologies Corp.) and visualized with 500-nm dichroic mirror and 535/50-nm emission filters (Semrock). Forskolin (Cayman Chemical), TTX (Alomone Labs), VIP (Peptide Institute), MDL12330A (Sigma-Aldrich), an agonist of adenosine (IB-MECA, Tocris Bioscience), an antagonist of VPAC2 receptors (PG99-465, Bachem), and an antagonist of adenosine A2A

receptors (ZM241385, Sigma-Aldrich) were dissolved in water or DMSO. These chemicals were then added to the culture medium.

Optical manipulation of cAMP in the SCN slice

To manipulate intracellular cAMP using bPAC, we used an LED array system (470 nm; LEDA-B, BRC). To manipulate cAMP into the SCN slice by blue light (frequency, 10 Hz; duration, 20 ms; intensity, 0.3 mW/mm^2), a pulse generator (STOmk-2) was connected to an LED driver. The stimulation was performed for 1 hour at 36.0°C. We measured PER2::LUC rhythms of the SCN slice for several days, and then, the culture dishes were moved onto the LED array to apply blue light. After blue light stimulation, the dishes were returned to a photon-counting device. We performed optical manipulation of cAMP up to three times in each SCN slice.

Virus injection and stereotaxic surgery

The mice (2 to 5 months old) were anesthetized with isoflurane (induction dose of ~2.5% and maintenance dose of ~1%) and placed in a stereotaxic instrument (David Kopf Instruments). We injected 120 nl of AAV (AAV-hSyn-flex-bPAC-2A-mCherry, 4.8×10^{12} genome copies/ml; AAV-CMV-flex-tdTomato, 2.8×10^{12} genome copies/ml) into the SCN (anteroposterior (AP), ±0.0 mm; mediolateral (ML), ±0.2 mm; dorsoventral (DV), −5.8 mm) with a glass micropipette and an air pressure injection system (BJ-110, BEX) (*17*). After infusion, the glass micropipette was left in place for at least 8 min. More than 2 weeks after AAV injection, we anesthetized the mice again and stereotaxically inserted an optical fiber [400-μm-diameter core; 0.39 numerical aperture (NA); Kyocera] just above the SCN (AP, ±0.0 mm; ML, ±0.0 mm; DV, −5.5 mm), and the fiber was fixed with dental cement. Carprofen (20 mg/kg; Zoetis Inc., Japan) was administered on the day of surgery for its anti-inflammatory and analgesic properties. After surgery, the mice were housed separately for at least 7 days before the start of locomotor activity measurements.

Optical manipulation of cAMP in the SCN in vivo

A flexible fiber-optic cable (BFYL4LS01; 400-μm-diameter core; 0.39 NA; Thorlabs) was connected to an optical fiber implanted in the mice, and the cable was attached to an LED light source (470 nm; 5 mW at the tip of the fiber; Thorlabs) as previously reported (*17*). To manipulate cAMP into SCN neurons by blue light (frequency, 10 Hz; duration, 20 ms), a pulse generator was connected to an LED driver. The stimulation was performed for 1 hour (from 1200 or 1300) every 24 hours under DD.

Measurement of locomotor activity

We measured the spontaneous movement of mice with a passive infrared sensor that detects changes in animal thermal radiation due to movement. Mice were housed individually in polycarbonate cages placed in a light-tight and air-conditioned box. The amount of movement was recorded every minute using a computer software (ClockLab, Actimetrics) (*17*).

Histological study

After recording locomotor activity, mice were anesthetized with isoflurane and perfused with saline, followed by a 10% formalin solution (Wako). Brains were extracted and postfixed in the same solution for 24 hours at 4°C, followed by 30% sucrose solution at 4°C for at least 2 days. Forty-micrometer coronal sections of the SCN were prepared using a cryostat (Leica CM3050S; Leica Microsystems) and stored at 4°C in phosphate-buffered saline (PBS). Immunostaining was performed as previously described (*17*). Briefly, brain sections were immersed in blocking buffer (1% bovine serum albumin and 0.25% Triton X-100 in PBS) and incubated with primary antibodies at 4°C overnight. The sections were washed with blocking buffer and incubated with secondary antibodies at 4°C overnight. The brain sections were counterstained with 4′,6-diamidino-2-phenylindole, mounted, and examined under a confocal microscope (LSM 710, Carl Zeiss AG). The primary antibody was mouse anti-mCherry (1:500 dilution; Sigma-Aldrich), and the secondary antibody was CF 594–conjugated donkey anti-mouse antibody (1:1000 dilution; Biotium). If the mCherry signal was barely detectable in the SCN under an optical fiber tract, then it was defined as expression failure.

Data analysis

Bioluminescence records of the first 12 hours were not used for rhythm analyses because of an initial high level of bioluminescence. The raw bioluminescence data obtained from the PMT were smoothed using a five-point moving average method and then detrended using a 24-hour running average subtraction method. The circadian amplitude was defined as the difference between the peak and trough in a circadian cycle and standardized by the peak level as described previously (*19*). The properties of circadian rhythm in bioluminescence and fluorescence signals at the pixel level (2.3 μm by 2.3 μm) were analyzed using a cosine curve fitting method as described previously (*21*, *38*). The dorsal, middle, and ventral areas of the SCN were separated by lines drawn every one-third between the dorsal and ventral edges. The 48-hour raw data were applied to curve fitting after subtracting the linear trend. The background level was calculated using the region of interest outside the SCN for each slice and was defined as the mean plus 5 × SD. The significance of the curve fitting was evaluated using the percent rhythm analysis (*56*). The acrophase of the circadian rhythm in the SCN was estimated from the best-fitted cosine curve and expressed as heatmaps. The percent rhythm indicates the variability estimated by the cosine regression and was expressed as a percentage of the total variability of raw data. To calculate the magnitude of the phase shifts, the acrophase of the PER2::LUC rhythms was calculated from the best-fitted cosine curve. The magnitude of the phase shift in response to optical manipulation of cAMP was then calculated as the differences between the phase predicted by forward extrapolation of the regression line obtained from the acrophase of the data before optical manipulation and the first acrophase after manipulation. The circadian period of behavioral rhythms under DD was calculated using a linear regression line through activity onsets (ClockLab, Actimetrics).

Statistics

We performed the following statistical analyses in Prism 8.0 (GraphPad): Student's *t*-test, Mann-Whitney *U* test, paired *t*-test, one-sample *t*-test, one-way analysis of variance (ANOVA), one-way repeated measures ANOVA, two-way repeated measures ANOVA, mixed-effects model test, Sidak's multiple comparisons test, Bonferroni's multiple comparisons test, and Tukey-Kramer test. A Rayleigh plot analysis was performed using the Oriana4 software (Kovach Computing Service). Data are expressed as means ± SD.

Supplementary Materials

This PDF file includes:
Figs. S1 to S8

Other Supplementary Material for this manuscript includes the following:
Movies S1 to S5

View/request a protocol for this paper from *Bio-protocol*.

REFERENCES AND NOTES

1. S. M. Reppert, D. R. Weaver, Coordination of circadian timing in mammals. *Nature* **418**, 935–941 (2002).
2. A. C. Liu, D. K. Welsh, C. H. Ko, H. G. Tran, E. E. Zhang, A. A. Priest, E. D. Buhr, O. Singer, K. Meeker, I. M. Verma, F. J. Doyle III, J. S. Takahashi, S. A. Kay, Intercellular coupling confers robustness against mutations in the SCN circadian clock network. *Cell* **129**, 605–616 (2007).
3. D. K. Welsh, D. E. Logothetis, M. Meister, S. M. Reppert, Individual neurons dissociated from rat suprachiasmatic nucleus express independently phased circadian firing rhythms. *Neuron* **14**, 697–706 (1995).
4. S. Yamaguchi, H. Isejima, T. Matsuo, R. Okura, K. Yagita, M. Kobayashi, H. Okamura, Synchronization of cellular clocks in the suprachiasmatic nucleus. *Science* **302**, 1408–1412 (2003).
5. E. D. Herzog, S. J. Aton, R. Numano, Y. Sakaki, H. Tei, Temporal precision in the mammalian circadian system: A reliable clock from less reliable neurons. *J. Biol. Rhythms* **19**, 35–46 (2004).
6. S. Honma, W. Nakamura, T. Shirakawa, K.-i. Honma, Diversity in the circadian periods of single neurons of the rat suprachiasmatic nucleus depends on nuclear structure and intrinsic period. *Neurosci. Lett.* **358**, 173–176 (2004).
7. M. J. Berridge, R. F. Irvine, Inositol trisphosphate, a novel second messenger in cellular signal transduction. *Nature* **312**, 315–321 (1984).
8. S. J. Aton, C. S. Colwell, A. J. Harmar, J. Waschek, E. D. Herzog, Vasoactive intestinal polypeptide mediates circadian rhythmicity and synchrony in mammalian clock neurons. *Nat. Neurosci.* **8**, 476–483 (2005).
9. E. S. Maywood, J. E. Chesham, J. A. O'Brien, M. H. Hastings, A diversity of paracrine signals sustains molecular circadian cycling in suprachiasmatic nucleus circuits. *Proc. Natl. Acad. Sci. U.S.A.* **108**, 14306–14311 (2011).
10. E. S. Maywood, A. B. Reddy, G. K. Y. Wong, J. S. O'Neill, J. A. O'Brien, D. G. McMahon, A. J. Harmar, H. Okamura, M. H. Hastings, Synchronization and maintenance of timekeeping in suprachiasmatic circadian clock cells by neuropeptidergic signaling. *Curr. Biol.* **16**, 599–605 (2006).
11. G. B. Lundkvist, Y. Kwak, E. K. Davis, H. Tei, G. D. Block, A calcium flux is required for circadian rhythm generation in mammalian pacemaker neurons. *J. Neurosci.* **25**, 7682–7686 (2005).
12. J. S. O'Neill, E. S. Maywood, J. E. Chesham, J. S. Takahashi, M. H. Hastings, cAMP-dependent signaling as a core component of the mammalian circadian pacemaker. *Science* **320**, 949–953 (2008).
13. R. Enoki, S. Kuroda, D. Ono, M. T. Hasan, T. Ueda, S. Honma, K.-i. Honma, Topological specificity and hierarchical network of the circadian calcium rhythm in the suprachiasmatic nucleus. *Proc. Natl. Acad. Sci. U.S.A.* **109**, 21498–21503 (2012).
14. M. Ikeda, T. Sugiyama, C. S. Wallace, H. S. Gompf, T. Yoshioka, A. Miyawaki, C. N. Allen, Circadian dynamics of cytosolic and nuclear Ca^{2+} in single suprachiasmatic nucleus neurons. *Neuron* **38**, 253–263 (2003).
15. T. Noguchi, T. L. Leise, N. J. Kingsbury, T. Diemer, L. L. Wang, M. A. Henson, D. K. Welsh, Calcium circadian rhythmicity in the suprachiasmatic nucleus: Cell autonomy and network modulation. *eNeuro* **4**, ENEURO.0160–ENEU17.2017 (2017).
16. M. Ikeda, M. Ikeda, Bmal1 is an essential regulator for circadian cytosolic Ca^{2+} rhythms in suprachiasmatic nucleus neurons. *J. Neurosci.* **34**, 12029–12038 (2014).
17. D. Ono, Y. Mukai, C. J. Hung, S. Chowdhury, T. Sugiyama, A. Yamanaka, The mammalian circadian pacemaker regulates wakefulness via CRF neurons in the paraventricular nucleus of the hypothalamus. *Sci. Adv.* **6**, eabd0384 (2020).
18. T. Sugiyama, H. Suzuki, T. Takahashi, Light-induced rapid Ca^{2+} response and MAPK phosphorylation in the cells heterologously expressing human OPN5. *Sci. Rep.* **4**, 5352 (2014).
19. D. Ono, S. Honma, K.-i. Honma, Cryptochromes are critical for the development of coherent circadian rhythms in the mouse suprachiasmatic nucleus. *Nat. Commun.* **4**, 1666 (2013).
20. M. H. Hastings, E. S. Maywood, J. S. O'Neill, Cellular circadian pacemaking and the role of cytosolic rhythms. *Curr. Biol.* **18**, R805–R815 (2008).
21. D. Ono, S. Honma, K.-i. Honma, Differential roles of AVP and VIP signaling in the postnatal changes of neural networks for coherent circadian rhythms in the SCN. *Sci. Adv.* **2**, e1600960 (2016).
22. A. B. Webb, N. Angelo, J. E. Huettner, E. D. Herzog, Intrinsic, nondeterministic circadian rhythm generation in identified mammalian neurons. *Proc. Natl. Acad. Sci. U.S.A.* **106**, 16493–16498 (2009).
23. E. E. Abrahamson, R. Y. Moore, Suprachiasmatic nucleus in the mouse: Retinal innervation, intrinsic organization and efferent projections. *Brain Res.* **916**, 172–191 (2001).
24. S. An, R. P. Irwin, C. N. Allen, C. Tsai, E. D. Herzog, Vasoactive intestinal polypeptide requires parallel changes in adenylate cyclase and phospholipase C to entrain circadian rhythms to a predictable phase. *J. Neurophysiol.* **105**, 2289–2296 (2011).
25. H. Wang, T. Qian, Y. Zhao, Y. Zhuo, C. Wu, T. Osakada, P. Chen, H. Ren, Y. Yan, L. Geng, S. Fu, L. Mei, G. Li, L. Wu, Y. Jiang, W. Qian, W. Peng, M. Xu, J. Hu, L. Chen, C. Tang, D. Lin, J.-N. Zhou, Y. Li, A toolkit of highly selective and sensitive genetically encoded neuropeptide sensors. bioRxiv 485911 [Preprint]. 28 March 2022. https://www.biorxiv.org/content/10.1101/2022.03.26.485911v1.
26. A. Jagannath, N. Varga, R. Dallmann, G. Rando, P. Gosselin, F. Ebrahimjee, L. Taylor, D. Mosneagu, J. Stefaniak, S. Walsh, T. Palumaa, S. di Pretoro, H. Sanghani, Z. Wakaf, G. C. Churchill, A. Galione, S. N. Peirson, D. Boison, S. A. Brown, R. G. Foster, S. R. Vasudevan, Adenosine integrates light and sleep signalling for the regulation of circadian timing in mice. *Nat. Commun.* **12**, 2113 (2021).
27. M. Stierl, P. Stumpf, D. Udwari, R. Gueta, R. Hagedorn, A. Losi, W. Gärtner, L. Petereit, M. Efetova, M. Schwarzel, T. G. Oertner, G. Nagel, P. Hegemann, Light modulation of cellular cAMP by a small bacterial photoactivated adenylyl cyclase, bPAC, of the soil bacterium *Beggiatoa*. *J. Biol. Chem.* **286**, 1181–1188 (2011).
28. M. Doi, A. Ishida, A. Miyake, M. Sato, R. Komatsu, F. Yamazaki, I. Kimura, S. Tsuchiya, H. Kori, K. Seo, Y. Yamaguchi, M. Matsuo, J.-M. Fustin, R. Tanaka, Y. Santo, H. Yamada, Y. Takahashi, M. Araki, K. Nakao, S. Aizawa, M. Kobayashi, K. Obrietan, G. Tsujimoto, H. Okamura, Circadian regulation of intracellular G-protein signalling mediates intercellular synchrony and rhythmicity in the suprachiasmatic nucleus. *Nat. Commun.* **2**, 327 (2011).
29. R. A. Prosser, M. U. Gillette, Cyclic changes in cAMP concentration and phosphodiesterase activity in a mammalian circadian clock studied in vitro. *Brain Res.* **568**, 185–192 (1991).
30. E. Morioka, Y. Kasuga, Y. Kanda, S. Moritama, H. Koizumi, T. Yoshikawa, N. Miura, M. Ikeda, H. Higashida, T. C. Holmes, M. Ikeda, Mitochondrial LETM1 drives ionic and molecular clock rhythms in circadian pacemaker neurons. *Cell Rep.* **39**, 110787 (2022).
31. M. Brancaccio, E. S. Maywood, J. E. Chesham, A. S. Loudon, M. H. Hastings, A Gq-Ca^{2+} axis controls circuit-level encoding of circadian time in the suprachiasmatic nucleus. *Neuron* **78**, 714–728 (2013).
32. J. R. Jones, T. Simon, L. Lones, E. D. Herzog, SCN VIP neurons are essential for normal light-mediated resetting of the circadian system. *J. Neurosci.* **38**, 7986–7995 (2018).
33. K. Shinohara, S. Honma, Y. Katsuno, H. Abe, K. Honma, Two distinct oscillators in the rat suprachiasmatic nucleus in vitro. *Proc. Natl. Acad. Sci. U.S.A.* **92**, 7396–7400 (1995).
34. B. Carpenter, R. Nehme, T. Warne, A. G. Leslie, C. G. Tate, Structure of the adenosine A_{2A} receptor bound to an engineered G protein. *Nature* **536**, 104–107 (2016).
35. Z.-L. Huang, Y. Urade, O. Hayaishi, The role of adenosine in the regulation of sleep. *Curr. Top. Med. Chem.* **11**, 1047–1057 (2011).
36. A. P. Patton, M. D. Edwards, N. J. Smyllie, R. Hamnett, J. E. Chesham, M. Brancaccio, E. S. Maywood, M. H. Hastings, The VIP-VPAC2 neuropeptidergic axis is a cellular pacemaking hub of the suprachiasmatic nucleus circadian circuit. *Nat. Commun.* **11**, 3394 (2020).
37. R. A. Prosser, M. U. Gillette, The mammalian circadian clock in the suprachiasmatic nuclei is reset in vitro by cAMP. *J. Neurosci.* **9**, 1073–1081 (1989).
38. D. Ono, S. Honma, Y. Nakajima, S. Kuroda, R. Enoki, K.-i. Honma, Dissociation of *Per1* and *Bmal1* circadian rhythms in the suprachiasmatic nucleus in parallel with behavioral outputs. *Proc. Natl. Acad. Sci. U.S.A.* **114**, E3699–E3708 (2017).
39. M. J. Vansteensel, S. Yamazaki, H. Albus, T. Deboer, G. D. Block, J. H. Meijer, Dissociation between circadian Per1 and neuronal and behavioral rhythms following a shifted environmental cycle. *Curr. Biol.* **13**, 1538–1542 (2003).
40. M. Doi, I. Murai, S. Kunisue, G. Setsu, N. Uchio, R. Tanaka, S. Kobayashi, H. Shimatani, H. Hayashi, H.-W. Chao, Y. Nakagawa, Y. Takahashi, Y. Hotta, J. I. Yasunaga, M. Matsuoka, M. H. Hastings, H. Kiyonari, H. Okamura, Gpr176 is a Gz-linked orphan G-protein-coupled receptor that sets the pace of circadian behaviour. *Nat. Commun.* **7**, 10583 (2016).
41. E. E. Zhang, Y. Liu, R. Dentin, P. Y. Pongsawakul, A. C. Liu, T. Hirota, D. A. Nusinow, X. Sun, S. Landais, Y. Kodama, D. A. Brenner, M. Montminy, S. A. Kay, Cryptochrome mediates circadian regulation of cAMP signaling and hepatic gluconeogenesis. *Nat. Med.* **16**, 1152–1156 (2010).

42. C. S. Colwell, S. Michel, J. Itri, W. Rodriguez, J. Tam, V. Lelievre, Z. Hu, X. Liu, J. A. Waschek, Disrupted circadian rhythms in VIP- and PHI-deficient mice. *Am. J. Physiol. Regul. Integr. Comp. Physiol.* **285**, R939–R949 (2003).
43. Z. Travnickova-Bendova, N. Cermakian, S. M. Reppert, P. Sassone-Corsi, Bimodal regulation of mPeriod promoters by CREB-dependent signaling and CLOCK/BMAL1 activity. *Proc. Natl. Acad. Sci. U.S.A.* **99**, 7728–7733 (2002).
44. K. Obrietan, S. Impey, D. Smith, J. Athos, D. R. Storm, Circadian regulation of cAMP response element-mediated gene expression in the suprachiasmatic nuclei. *J. Biol. Chem.* **274**, 17748–17756 (1999).
45. E. S. Maywood, L. Drynan, J. E. Chesham, M. D. Edwards, H. Dardente, J.-M. Fustin, D. G. Hazlerigg, J. S. O'Neill, G. F. Codner, N. J. Smyllie, M. Brancaccio, M. H. Hastings, Analysis of core circadian feedback loop in suprachiasmatic nucleus of mCry1-luc transgenic reporter mouse. *Proc. Natl. Acad. Sci. U.S.A.* **110**, 9547–9552 (2013).
46. R. Enoki, D. Ono, S. Kuroda, S. Honma, K.-i. Honma, Dual origins of the intracellular circadian calcium rhythm in the suprachiasmatic nucleus. *Sci. Rep.* **7**, 41733 (2017).
47. C. H. Ko, Y. R. Yamada, D. K. Welsh, E. D. Buhr, A. C. Liu, E. E. Zhang, M. R. Ralph, S. A. Kay, D. B. Forger, J. S. Takahashi, Emergence of noise-induced oscillations in the central circadian pacemaker. *PLOS Biol.* **8**, e1000513 (2010).
48. M. Nakajima, K. Imai, H. Ito, T. Nishiwaki, Y. Murayama, H. Iwasaki, T. Oyama, T. Kondo, Reconstitution of circadian oscillation of cyanobacterial KaiC phosphorylation in vitro. *Science* **308**, 414–415 (2005).
49. J. Tomita, M. Nakajima, T. Kondo, H. Iwasaki, No transcription-translation feedback in circadian rhythm of KaiC phosphorylation. *Science* **307**, 251–254 (2005).
50. J. S. O'Neill, A. B. Reddy, Circadian clocks in human red blood cells. *Nature* **469**, 498–503 (2011).
51. J. S. O'Neill, G. van Ooijen, L. E. Dixon, C. Troein, F. Corellou, F.-Y. Bouget, A. B. Reddy, A. J. Millar, Circadian rhythms persist without transcription in a eukaryote. *Nature* **469**, 554–558 (2011).
52. S. Wu, S. Esumi, K. Watanabe, J. Chen, K. C. Nakamura, K. Nakamura, K. Kometani, N. Minato, Y. Yanagawa, K. Akashi, K. Sakimura, T. Kaneko, N. Tamamaki, Tangential migration and proliferation of intermediate progenitors of GABAergic neurons in the mouse telencephalon. *Development* **138**, 2499–2509 (2011).
53. L. Vong, C. Ye, Z. Yang, B. Choi, S. Chua Jr., B. B. Lowell, Leptin action on GABAergic neurons prevents obesity and reduces inhibitory tone to POMC neurons. *Neuron* **71**, 142–154 (2011).
54. S. H. Yoo, S. Yamazaki, P. L. Lowrey, K. Shimomura, C. H. Ko, E. D. Buhr, S. M. Siepka, H.-K. Hong, W. J. Oh, O. J. Yoo, M. Menaker, J. S. Takahashi, PERIOD2::LUCIFERASE real-time reporting of circadian dynamics reveals persistent circadian oscillations in mouse peripheral tissues. *Proc. Natl. Acad. Sci. U.S.A.* **101**, 5339–5346 (2004).
55. N. Kon, H.-T. Wang, Y. S. Kato, K. Uemoto, N. Kawamoto, K. Kawasaki, R. Enoki, G. Kurosawa, T. Nakane, Y. Sugiyama, H. Tagashira, M. Endo, H. Iwasaki, T. Iwamoto, K. Kume, Y. Fukada, Na^+/Ca^{2+} exchanger mediates cold Ca^{2+} signaling conserved for temperature-compensated circadian rhythms. *Sci. Adv.* **7**, eabe8132 (2021).
56. W. Nelson, Y. L. Tong, J. K. Lee, F. Halberg, Methods for cosinor-rhythmometry. *Chronobiologia* **6**, 305–323 (1979).

Acknowledgments: We thank M. P. Butler and Y. Yamanaka for the valuable discussion of this study; S. Honma and K. Honma for providing experimental materials; J. S. Takahashi for supplying PER2::LUC mice; S. Kuroda for the analysis program of time-lapse images; and S. Nasu, S. Tsukamoto, and The Center for Animal Research and Education at Nagoya University for animal care. **Funding:** This work was supported by the Uehara Memorial Foundation, Kowa Life Science Foundation, Takeda Science Foundation, Kato Memorial Bioscience Foundation, DAIKO Foundation, SECOM Science and Technology Foundation, Research Foundation for Opto-Science and Technology, the Nakatani Foundation for Advancement of Measuring Technologies in Biomedical Engineering, Casio Science Promotion Foundation, Innovation inspired by Nature Research Support Program, SEKISUI CHEMICAL CO. LTD., Konica Minolta Science and Technology Foundation, the Inamori Foundation, Suntory Rising Stars Encouragement Program in Life Sciences (SunRiSE; to N.K.), the JST FOREST Program (grant number JPMJFR211A; Japan), and the JSPS KAKENHI (21K19255, 21H02526, 21H00307, 21H00422, 20KK0177, and 18H02477 to D.O.). **Author contributions:** D.O. designed the research. D.O., C.J.H., H.-t.W., N. K., and T.S. performed the experiments. H.W. and Y.L. made the GRAB sensor. T.S. made the bioluminescence probe. A.Y. provided support for AAV production, and D.O. wrote the manuscript. **Competing interests:** The authors declare that they have no competing interests. **Data and materials availability:** All data needed to evaluate the conclusions in the paper are present in the paper and/or the Supplementary Materials. Vgat-IRES-Cre and PER2::LUC mice are available from B. Lowell and J. Takahashi under a material transfer agreement with Beth Israel Deaconess Medical Center and Northwestern University, respectively. bPAC is also available from P. Hegemann under a material agreement with Humboldt University.

Submitted 25 April 2022
Accepted 23 November 2022
Published 4 January 2023
10.1126/sciadv.abq7032

ScienceAdvances

Network-driven intracellular cAMP coordinates circadian rhythm in the suprachiasmatic nucleus

Daisuke OnoHuan WangChi Jung HungHsin-tzu WangNaohiro KonAkihiro YamanakaYulong LiTakashi Sugiyama

Sci. Adv., 9 (1), eabq7032. • DOI: 10.1126/sciadv.abq7032

Science Advances (ISSN) is published by the American Association for the Advancement of Science. 1200 New York Avenue NW, Washington, DC 20005. The title *Science Advances* is a registered trademark of AAAS.